RSC Advances

ROYAL SOCIETY OF CHEMISTRY

www.rsc.org/advances

Journal Name

Dynamic Article Links ►

Cite this: DOI: 10.1039/c0xx00000x

www.rsc.org/xxxxxx

ARTICLE TYPE

Facile reversible LSPR tuning through additive-induced self-aggregation and dissemination of Ag NPs: Role of cyclodextrins and surfactants

Niharendu Mahapatra and Mintu Halder*

Received (in XXX, XXX) Xth XXXXXXXXX 20XX, Accepted Xth XXXXXXXXX 20XX
DOI: 10.1039/b000000x

Tuning the optoelectronic properties by controlling coupled surface plasmon modes in metal nanomaterials is one of the major challenges. Several methods have been developed for localized surface plasmon resonance (LSPR) tuning, which are generally provoked by the self-assembly of certain molecule (e.g. protein, viologen etc.) causing aggregation of nanoparticles. Here, we have developed a new and simple method applied on dilute cetyltrimethylammonium bromide (CTAB) stabilized Ag NPs for reversible LSPR tuning through additive-induced formation and subsequent dispersion of self-aggregates. Addition of cyclodextrin (α– or β–) results in decrease of surface charge of NPs, by taking away CTAB out of nanoparticle surface, through formation of inclusion complex. The slow formation of self-aggregates of Ag NPs is due to the gradual decrease in surface charge which results a large red-shifting of the LSPR band (436 nm - 537 nm). On subsequent addition of different types of surfactants alters the surface charge by re-attachment of stabilizer and results in the dispersion of self-aggregates with blue-shifting of LSPR band (537 nm - 420 nm). This efficient formation and break down of self-aggregates are monitored by dynamic light scattering (DLS) and transmission electron microscopy (TEM) measurements also and are correlated with alteration of the plasmonic absorption band. Variation in surface charge of Ag NPs is followed by zeta-potential measurements. This easy approach to control the plasmon absorption position can be very significant in sensing, optoelectronic devices etc.

Cite this: DOI: 10.1039/c0xx00000x

www.rsc.org/xxxxxx

ARTICLE TYPE

1. Introduction

During the past two decades there is a growing research interest in the field of various metal nanomaterials due to their unique optical, electrical, and magnetic properties for broad applications in optoelectronics, catalysis, sensors, and therapeutics[1-5]. Appearance of localized surface plasmon resonance (LSPR) is one of the most interesting phenomena of the nanosized metal nanomaterials[6]. The electric field of the electromagnetic radiation causes a collective coherent oscillation of the conductive electrons in nanomaterials at the interface of metal and dielectric. Such oscillating resonance is known as LSPR, appears in the visible region for noble metals such as silver and gold. Control of light at the nanoscale using surface plasmons[7] encompasses various unique optical phenomena such as enhancement of localized electromagnetic (EM) field at nanostructured metal surface,[8] extraordinary sensitivity of the LSPR to external medium,[9] high transmission through sub-wavelength apertures in thin metal film[10, 11]. LSPR is of enormous interest due to their potential applications in plasmonic circuits[12, 13], photovoltaics[14, 15] and chemical/biological sensors[16]. Various factors are responsible for LSPR of metal nanostructures, such as composition, size, shape, dielectric ambient and proximity to other nanoparticle (plasmon coupling)[17, 18].

Tuning of LSPR along with the plasmonic properties of metal nanostructures and their assemblies is a growing challenge because of their potential applications in sensing, optoelectronics and photonics. Formation of aggregates of the nanostructures, either solution condition or nanoparticle surface modification[19], is a reliable way for LSPR tuning as the plasmon coupling strength decays exponentially with separation[20]. The distance of separation between the nanostructures is highly dependent on the extent of aggregation.

The phenomenon of aggregation of the particles in a colloid solution can be brought about by various means, e.g., (i) upon addition of a "self-assembling" molecule or, (ii) modulation of surface charge of the nanoparticles. The aggregation process starts with a color change, which is eventually followed by the precipitation of the nanoparticles. This type of precipitation, due to over-aggregation, is a nuisance to the scientist who would like to have the stable aggregated colloid for various applications; e.g. surface enhanced Raman scattering (SERS)[21, 22] or surface plasmon spectroscopy (SPS)[23]. Several possibilities have been explored in obtaining the stable aggregated colloid in controlled way. Organic molecule, macromolecular scaffolds and biomolecules such as polymers[24], dendrimers[25], multi-dentate thioethers[26] and proteins[27] are used as self-assembling molecules for the formation of stable aggregated nanosol. Poly(amidoamine) (PAMAM) dendrimer has been used to tune Au-nanoparticle interparticle spacing by varying size of the dendrimers[25]. Alternatively, lysozyme has been employed as a model protein to control the interparticle spacing by changing the molar ratio of protein to Au-nanoparticle or by controlling the assembly temperature[27]. Previous literature reports reveal that carboxylate-functionalized nanosols or carboxylate-containing-DNA-functionalized colloids display aggregation behavior as a function of pH and metal ion concentration[28-30]. At high pH (complete deprotonation of carboxyl group) the particles in the colloid remain separated, but lowering of the pH leads to aggregation due to protonation of some carboxylic functions, allowing interactions between the particles. The extent of aggregation can often be controlled by reaching the appropriate pH of the colloidal solution. Binding of heavy metals with carboxylate group lowers the surface charge of the nanoparticles causing aggregation. This type of aggregation process can be employed to monitor the heavy metal ion level for water treatment[29, 30]. Similar type of controlled and stable aggregates of Au-nanoparticles has been achieved by varying the pH of poly (4-vinyl pyridine) (P4VP) polymer film[31]. The aggregation and dispersion of Au-nanoparticles occur because of pH responsive coiled and extended state of the polymer chain. Again reversible aggregation of DNA-coated colloids has been observed for which the temperature of the single particle-aggregate transition is indicative of the degree of DNA complementarity[32]. However, in most of the cases the self-assembling molecule becomes inserted between the nanoparticles during aggregation process, i.e., one extra molecule remains incorporated within the nano-assemblies, which can causes complication for further studies while using these aggregated nanoparticles.

Herein, for the first time, we have demonstrated a facile strategy for the reversible tunability of LSPR through additive-induced formation and subsequent dispersion of self-aggregates of dilute cetyltrimethylammonium bromide (CTAB) stabilized silver nanoparticles (Ag NPs). The LSPR of Ag NPs gets red-shifted by the addition of cyclodextrin (CDx) to the silver colloid possibly be due to self-aggregation of the nanoparticles. Addition of surfactants to cyclodextrin pre-treated Ag NP sample can stop and also lead to blue-shifting of LSPR band through break down of self-aggregates. NPs get stabilized and well dispersed in solution as colloid due to the surface charge. In the case of our NPs the surface charge (causing a "ζ-potential") is provided by the stabilizer surfactant molecules adhering to the surface. Now the decrease of surface charge, as a result of removal of those surfactants, lowers the ζ-potential leading to NP-aggregation. Upon re-attachment of ionic surfactant on the surface can increase the ζ-potential causing dissemination of NP. Thus the well controlled surface charge plays leading role for the formation and subsequent dispersion of self-aggregates of Ag NPs. Again, surfactants of different charge-type can lead to different inherent properties of nanoparticles such as structural stability, adsorption characteristics, surface charge, reshaping and redistribution of particles morphology. The method allows an efficient and cost-effective tool for the generation of stable nano-aggregates without insertion of any self-assembling molecule, which could pave the way for creation of new materials for applicative reasons.

Here we use surfactants having different charge-type head groups (namely, positive, negative and neutral) for the reversal of LSPR position (blue shifting) which ought to modify the surface charge of NPs and this will be evident from zeta-potential measurements. This well tuned surface charge of nanoparticles plays dominating role in binding, disrupting, and penetrating through many proteins, DNA, and cell-membrane as the interactions of these systems with nanoparticles are predominantly electrostatic in nature. The interaction of HSA with the nanoparticles is also predominantly electrostatic, and interestingly the protein concentration for stabilization of the conjugates decreases when the overall negative charge on the nanoparticle surface increases[33]. Positive surface charge on nanoparticle is efficient for absorption and negative surface charge on nanoparticle is found to be efficient for desorption of DNA[34]. Again positively charged nanoparticles can bind, disrupt and penetrate the cell membranes to the greatest extent, while neutral, negative, and zwitterionic NPs have negligible effects[35, 36]. It has been reported that hydroxyapatite (HAP) nanoparticle-induced aggregation of the red blood cells (RBCs) occurs *via* the electrostatic interaction between the positively charged binding sites on the HAP surface and the negatively charged groups on the surface of the RBCs[37]. The surface charge of nanoparticles can be crucial for drug/fluorescent-probe carrier systems, because many proteins, DNA, and cell-membrane surfaces are slightly anionic[38].

2. Materials and Methods

2.1 Materials

Purest grade carmoisine, silver nitrate ($AgNO_3$), cetyltrimethylammonium bromide (CTAB), cetylpyridinium chloride (CpCl), Triton X-100 (Tx-100), sodium dodecyl sulfate (SDS), sodium dodecylbenzene sulfonate (SDBS), α, β and γ cyclodextrin are purchased from Sigma Aldrich. NaOH (AR grade) is purchased from Merck. The whole experiment is performed in deionized triply distilled water. All glasswares are cleaned thoroughly by nitric acid and freshly prepared chromic acid, rinsed thoroughly with distilled water and acetone, and then dried in oven.

2.2. Instrumentation

Photochemical reaction is performed by using Xenon lamp from Newport model 66902 (300 watts) in a photo-reactor made up of a 100 ml round bottomed flask (made with borisilicate glass) with a magnetic stirrer. Light luminous flux per unit area is measured by using Lutron LX - 107HA digital light meter and the synthesis is performed at a light luminous flux per unit area of 50000 (±100) Lux. The pH measurements are carried out on a Eutech-510 ion pH-meter, which is pre-calibrated with standard pH buffer tablets. Electronic absorption spectra are recorded with a UV-2450 (Shimadzu) absorption spectrophotometer against solvent reference. Transmission electron microscopy (TEM) images are acquired using FEI-Tecnai G2 20 s-Twin with an operating voltage of 200 kV. Measurement of particle size distribution through dynamic light scattering (DLS) and surface charge of the nanoparticles by zeta potential is performed with a Malvern Nano ZS instrument employing a 4mW He-Ne laser operating at a wavelength of 632.8 nm and an avalanche photodiode (APD) detector.

2.3. Synthesis of Ag Nanostructures

Ag NP is prepared by our previous reported photochemical method[39]. In a typical procedure, 50 ml of the reaction mixture at pH 9.0 (made by adding drops of aqueous NaOH of 0.1M concentration) in a round bottom flask, containing dilute carmoisine (10μM), CTAB and $AgNO_3$ at a mole ratio of 1 : 5 : 5, are irradiated with broad band visible light from Xenon source using a light luminous flux per unit area of 50000 (±100) Lux at 25°C for 180 minutes with constant stirring using a magnetic stirrer. The Characteristic pale yellow colored silver sol is characterized by UV-VIS spectroscopy and TEM image.

2.4 UV-VIS spectroscopy, DLS, TEM and Zeta potential measurements

The additive-induced tuning of LSPR band, hydrodynamic radius, morphology and surface charge are monitored by UV-VIS spectroscopy, DLS, TEM and Zeta-potential measurements, respectively, for samples obtained by incubating the so-synthesized Ag NP solution for one hour after addition of 50μM of cyclodextrin (α, β and γ) to it. The same measurements are performed after addition of various concentrations of surfactants of different charge-type (CTAB, CpCl, Tx-100, SDS and SDBS) to the cyclodextrin-pretreated Ag NP sample. All the measurements are taken at various time intervals after addition of fixed concentration of CDx (0.05 mM) and the representative spectrum and / or images shown correspond to samples for 60 min interval only, and further to this sample different concentrations of a variety of surfactants are added and measurements are repeated.

3. Results and Discussion

Extinction spectra of our synthesized CTAB-stabilized silver nanoparticles show the characteristic plasmon absorption band at 436 nm. Figure 1A and 1B show the changes in extinction spectra and shifting of localized surface plasmon resonance (LSPR) peak position with time, respectively, of our so-synthesized Ag NPs in the absence and presence of 50μM α– or, β– or, γ–CDx. After addition of CDx, the extinction spectrum of the Ag NPs shift to longer wavelength with a concomitant change in color (pale yellow color discharges) with α– and β–CDx, but not for γ–CDx. The significant red shifting of LSPR band (to 537 nm for α-CDx and 474 nm for β-CDx) with time is attributed to the strong plasmon coupling of the self-aggregated Ag NPs[40]. This is also evident from DLS studies and TEM images as discussed later.

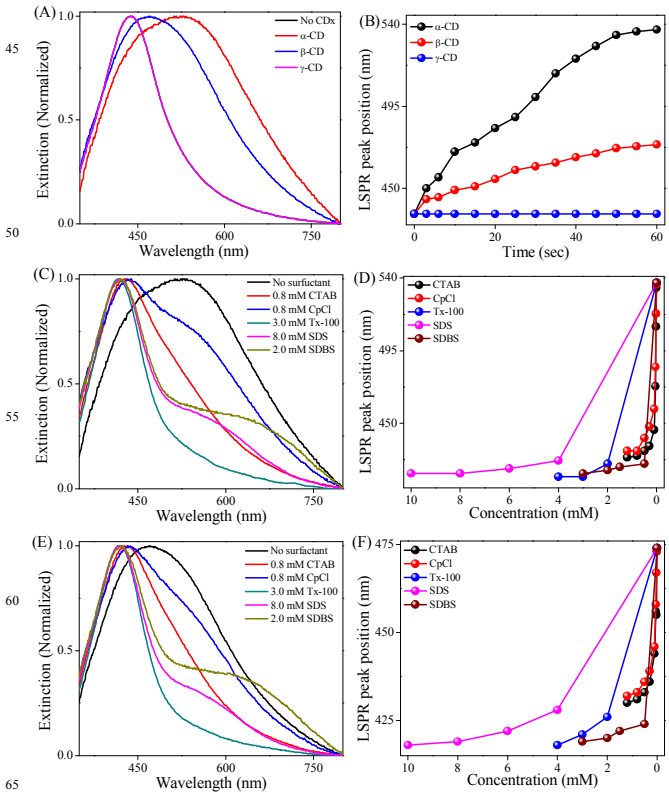

Figure 1. (A) UV-VIS extinction spectra and (B) LSPR peak position of Ag NPs in absence and presence of 50 μM α–, or β–, or γ–CDx with time. UV-VIS extinction spectra of (C) α– and (E) β–CDx pre-treated Ag NP sample in absence and presence of different concentrations of various surfactants. Plots of LSPR peak position of (D) α– and (F) β–CDx pre-treated Ag NP sample in absence and presence of different concentrations of various surfactants.

The shift in the LSPR band position can be arrested at any stage of time and also can be reverted back to its initial band position in the presence of different concentrations of surfactants (e.g. CTAB, CpCl, Tx-100, SDS and SDBS). Addition of surfactant leads to blue shifting of the initially CDx-induced red-shifted LSPR band (figure 1C and 1E) with consequent re-appearance of the pale yellow color. This blue-shifting of LSPR peak position (figure 1D and 1F) is attributed to be due to breaking of self-aggregates of Ag NPs as evident from DLS studies and recorded TEM images, and is discussed later. Here one point should be noted that the nature of concentration-dependent back-shifting depends on the charge-type of the head-group of surfactant used. Addition of a minimum concentration of positively charged surfactants (listed in table 1) can stop the time-dependent red-shifting of LSPR band to a certain position (see table 1) and further addition leads to reversal of LSPR position (blue-shifting). On the other hand, addition of a minimum

concentration of neutral or negatively charged surfactants (as shown in table 1) leads to sudden blue-shifting of LSPR band without any stoppage unlike cationic surfactants.

Table 1. List of minimum concentrations of different surfactants required to stop the CDx-induced LSPR shifting of Ag NPs at any time. The LSPR peak positions at the corresponding surfactant concentrations are also tabulated.

Surfactant	Charge on the head group	Minimum concentration (mM)	LSPR peak position for α/β–CDx (nm)
CTAB	Positive	0.01	534 / 473
CpCl	Positive	0.01	536 / 473
Tx-100	Neutral	2	425 / 426
SDS	Negative	4	427 / 428
SDBS	Negative	0.5	425 / 424

The DLS technique is utilized to monitor the change in hydrodynamic radius (R_h), and TEM imaging is employed to follow the morphological changes of CTAB-coated Ag NPs after additions of CDx and also for samples with subsequently added surfactants. Figure 2A and 2B exhibit gradual increase in hydrodynamic radius with time in absence and presence of 50μM α-or β-CDx. The average hydrodynamic radius of our synthesized Ag NPs is ~142 nm and after addition of CDx, it increases to ~827 nm and ~398 nm for α-CDx and β-CDx, respectively. On the other hand, TEM images reveals that initially our synthesized Ag NPs mostly exist as a distribution of stand-alone particles (figure 3A) and after addition of CDx (50 μM) the particles get aggregated (figure 3B and 3C). Thus the self-aggregation of NPs, as evident from the TEM images and the increase in hydrodynamic radius, appears to be a significant factor to large red-shifting the LSPR band with time. The LSPR band resulting from plasmon coupling of the self-aggregated nanoparticles is known as coupled plasmon band, the peak position of which depends on the extent of aggregation[31]. The greater extent of self-aggregation of Ag NPs in presence of α–CDx than β–CDx for same added concentration is accompanied by a larger red-shifting of LSPR band in the former. The broadening of LSPR band and DLS band-width due to CDx indicates the polydispersity of the nanoparticle aggregates, which is also evident from TEM images.

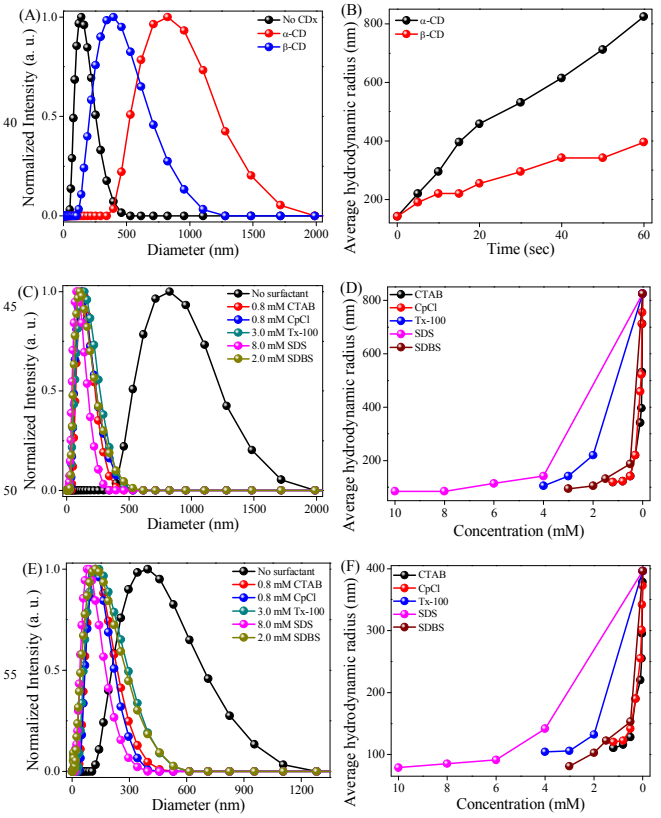

Figure 2. (A) DLS spectra and (B) average hydrodynamic radius (R_h) of Ag NPs in absence and presence of 50 μM α or β-CDx with time. DLS spectra of (C) α– and (E) β–CDx pre-treated Ag NP sample in absence and presence of different concentrations of various surfactants. Plots of average hydrodynamic radius (R_h) of (D) α– and (F) β–CDx pre-treated sample in absence and presence of different concentrations of various types of surfactants.

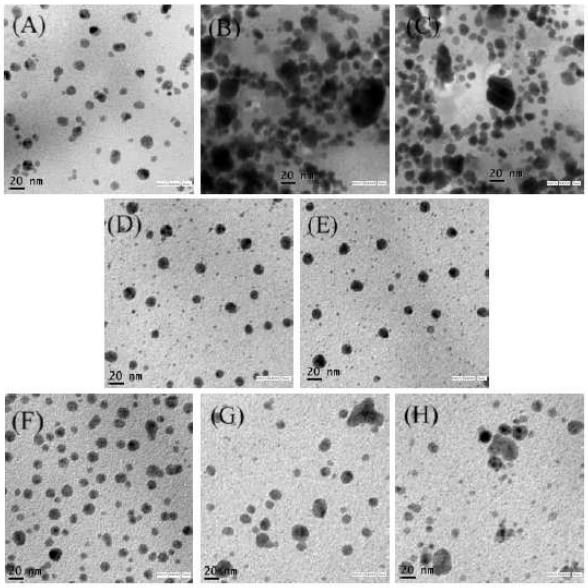

Figure 3. TEM images of Ag NPs in (A) absence and presence of 50 μM (B) α-CD and (C) β-CDx at 60 min. Representative TEM images of α-

CDx pre-treated Ag NP samples in presence of (D) 0.8 mM CTAB, (E) 0.8 mM CpCl, (F) 2 mM Tx-100, (G) 4 mM SDS and (H) 0.5 mM SDBS.

The DLS spectra of CDx induced self-aggregated Ag NP samples exhibit the concentration dependent gradual decrease in hydrodynamic radius with charged surfactants as additives; whereas sudden decrease in hydrodynamic radius is observed with neutral or negatively charged surfactants (figure 2C, 2D, 2E and 2F). TEM images of CDx pre-treated Ag NP samples in absence (figure 3B and 3C) and presence (images are not shown) of the minimum concentration (as mentioned in table1) of positively charged surfactants are comparable, but higher concentration leads to disaggregated particles as evident from TEM images 3D and 3E. On the other hand, addition of the minimum concentration (as mentioned in table 1) of neutral or negatively charged surfactants directly results in the disaggregated particles as shown in TEM images 3F, 3G and 3H. The TEM images of samples after addition of surfactants shows the decrease in polydispersity of the nanoparticles, which is correlated with the reduced LSPR band width and narrow DLS spectrum. Thus one can tune the LSPR band by controlling the self-aggregation process using our easy and economic protocol.

To investigate the possible mechanism behind CDx-assisted formation and subsequent surfactant-induced dispersion of self-aggregates of Ag NPs, we have performed zeta-potential (ζ) measurements. Figure 4A shows the variation of ζ-potential with time after addition of 50 μM α– or β–CDx. The ζ-potential of synthesized Ag NP is +21.2 mV (± 0.76), which decreases to +4.15 mV and +6.18 mV after addition of α– and β–CDx, respectively. Initially the high positive surface charge (+21.2 mV) is due to the presence of positively charged CTAB on the particle surface, which is responsible for the inter-particle repulsion in order to avoid the aggregation. The decrease in surface charge of Ag NPs in presence of CDx may be due to the (a) attachment of CDx on the particle surface[41] by removing surface attached stabilizer CTAB molecules; (b) insertion of CDx between nanoparticles through formation of inclusion complex with stabilizer molecules[42] and (c) detachment of CTAB from NP surface through inclusion complexation with CDx[43] (scheme 1). The surface charge will be negative for CDx stabilized Ag NPs at pH ≈ 8 (the pH of the initial Ag NP solution), due to the partial deprotonation of hydroxyl group of sugar-units at basic pH[41, 44]. The almost unchanged positive ζ-potential of CDx-treated sample after 60 min (figure 4A) negates the possibility of attachment of CDx on nanoparticle surface. Again replacement of CTAB from surface by CDx signifies its higher binding affinity for NPs. But increase of positive ζ-potential through subsequent addition of CTAB to CDx-induced aggregated Ag NPs (figure 4B and 4C) should correspond to reattachment of CTAB, which is contradictory to previously stated higher binding affinity of CDx for Ag NPs. Again, insertion of CDx between nanoparticles through formation of inclusion complex with surface stabilizer CTAB can lead to the decrease in ζ-potential through neutralization of positive charge of CTAB with partial negative charge of hydroxyl groups of CDx at pH ≈ 8, which reveals that the nanoparticles surface remains intact after addition of CDx. Thus subsequent addition of different surfactants to Ag NP-CDx mixture will simply take-away the inserted CDx through inclusion complexation, which results in the increase of positive ζ-potential for any types of surfactant due to the presence of unimpaired CTAB on NP's surface. But unchanged ζ-potential after addition of neutral surfactant, and some negative ζ-potential after addition of negatively charged surfactant head-group to Ag NP-CDx mixture (figure 4B and 4C) indicate that CTAB detaches from NP-surface through formation of inclusion complex with CDx. The detachment of CTAB from the surface is also manifested in the reshaping and resizing of the nanoparticles as shown in TEM images (figure 3). Hence the decrease in surface charges, due to detachment of CTAB from the NPs surface *via* inclusion complexation with CDx, results in the self-aggregation. The greater extent of self-aggregation in presence of α-CDx is correlated with the stronger inclusion complexation between CTAB and α-CDx than that of β-CDx[43, 45]. In the aforementioned aggregation process, there still remains a little amount of surface charge on the nano-aggregate, which makes them stable in solution[40]. The re-attachment of added surfactants on the CDx-modified Ag NPs surface results in the breaking of self-aggregates, presumably due to the increase in ζ-potential for charged surfactants and insertion of nanoparticles within the micelle for neutral surfactants (CMC of Tx-100 is 0.27 mM[46]). Thus we have demonstrated an easy and inexpensive protocol for the generation of controlled self-aggregated Ag NPs without insertion of any self-assembling molecule.

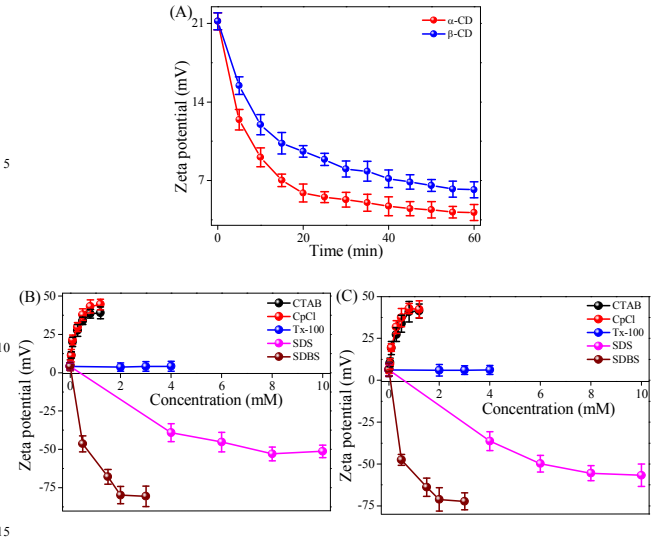

Figure 4. (A) Variation of zeta potential (ζ) of Ag NPs with time in presence of 50 μM α or β-CDx. Change in zeta potential (ζ) of (B) α– and (C) β–CDx pre-treated Ag NP sample in presence of different concentrations of various types of surfactants.

Scheme 1. Schematic representation of the formation and subsequent dispersion of self-aggregates of Ag NPs.

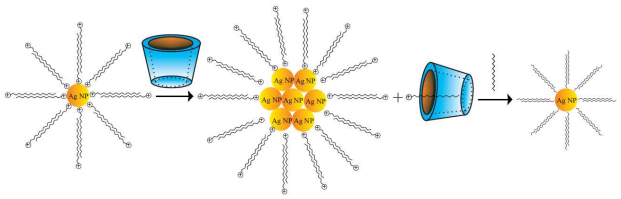

4. Conclusions

In conclusion, we have demonstrated an easy, simple and economically inexpensive protocol for reversible LSPR tuning through formation and subsequent dispersion of self-aggregates of nanoparticles in a controlled way. Modulation of surface charge of Ag NPs by the addition of CDx and subsequent addition of different surfactants is responsible for the formation and dispersion of self-aggregates. The detachment of CTAB from nanoparticles surface through inclusion complexation with CDx and subsequent reattachment of different surfactants on nanoparticles surface is responsible for surface charge modulation of Ag NPs. This surface-charge-controllability of nanoparticles with various altered surface charges, is significantly important in binding, disrupting, and penetrating with many proteins, DNA, and cell-membrane[33, 34, 37]. The simple and efficient method presented here enables large tunability in optical properties, which is significant for the application in developing highly sensitive chemical and biological sensors, optoelectronic devices and adaptive materials. Our approach is unique in the sense that we have been able to demonstrate shifting and reverse-shifting of LSPR band via external additives avoiding heavy metals unlike DNA-based systems as reported elsewhere[29, 30].

Abbreviation

Ag NP, silver nanoparticle; LSPR, localized surface plasmon resonance; CDx, cyclodextrin; CTAB, cetyltrimethylammonium bromide; CpCl, cetylpyridinium chloride; Tx-100, Triton X-100; SDS, sodium dodecyl sulfate; SDBS, sodium dodecylbenzene sulfonate; CMC, critical micellar concentration.

Acknowledgements

We thank DST SERB-India (Fund no. SB/S1/PC-041/2013) for financial support. NM thanks CSIR-India for his individual fellowship. We thank Prof. N. Sarkar for help in measuring DLS and ζ-potential in his lab-setup.

References

1. D. Chen, G. Wang and J. H. Li, *J Phys Chem C*, 2007, **111**, 2351-2367.
2. W. L. Cheng, S. J. Dong and E. K. Wang, *J Phys Chem B*, 2004, **108**, 19146-19154.
3. X. G. Hu and S. J. Dong, *J Mater Chem*, 2008, **18**, 1279-1295.
4. X. H. Huang, P. K. Jain, I. H. El-Sayed and M. A. El-Sayed, *Nanomedicine-Uk*, 2007, **2**, 681-693.
5. M. Seydack, *Biosens Bioelectron*, 2005, **20**, 2454-2469.
6. P. K. Jain, X. Huang, I. H. El-Sayed and M. A. El-Sayad, *Plasmonics*, 2007, **2**, 107-118.
7. E. Ozbay, *Science*, 2006, **311**, 189-193.
8. E. Hao and G. C. Schatz, *J Chem Phys*, 2004, **120**, 357-366.
9. K. A. Willets and R. P. Van Duyne, *Annu Rev Phys Chem*, 2007, **58**, 267-297.
10. W. L. Barnes, A. Dereux and T. W. Ebbesen, *Nature*, 2003, **424**, 824-830.
11. T. W. Ebbesen, H. J. Lezec, H. F. Ghaemi, T. Thio and P. A. Wolff, *Nature*, 1998, **391**, 667-669.
12. T. Nikolajsen, K. Leosson and S. I. Bozhevolnyi, *Appl Phys Lett*, 2004, **85**, 5833-5835.
13. W. S. Cai, J. S. White and M. L. Brongersma, *Nano Lett*, 2009, **9**, 4403-4411.
14. O. Stenzel, A. Stendal, K. Voigtsberger and C. Vonborczyskowski, *Sol Energ Mat Sol C*, 1995, **37**, 337-348.
15. H. A. Atwater and A. Polman, *Nat Mater*, 2010, **9**, 205-213.
16. J. N. Anker, W. P. Hall, O. Lyandres, N. C. Shah, J. Zhao and R. P. Van Duyne, *Nat Mater*, 2008, **7**, 442-453.
17. N. L. Rosi and C. A. Mirkin, *Chem Rev*, 2005, **105**, 1547-1562.
18. B. M. Reinhard, M. Siu, H. Agarwal, A. P. Alivisatos and J. Liphardt, *Nano Lett*, 2005, **5**, 2246-2252.

19. T. Ung, L. M. Liz-Marzan and P. Mulvaney, *J Phys Chem B*, 2001, **105**, 3441-3452.
20. P. K. Jain, W. Y. Huang and M. A. El-Sayed, *Nano Lett*, 2007, **7**, 2080-2088.
21. A. Campion and P. Kambhampati, *Chem Soc Rev*, 1998, **27**, 241-250.
22. M. Moskovits, *Rev Mod Phys*, 1985, **57**, 783-826.
23. P. Mulvaney, *Langmuir*, 1996, **12**, 788-800.
24. A. K. Boal and V. M. Rotello, *J Am Chem Soc*, 2002, **124**, 5019-5024.
25. B. L. Frankamp, A. K. Boal and V. M. Rotello, *J Am Chem Soc*, 2002, **124**, 15146-15147.
26. M. M. Maye, I. I. S. Lim, J. Luo, Z. Rab, D. Rabinovich, T. B. Liu and C. J. Zhong, *J Am Chem Soc*, 2005, **127**, 1519-1529.
27. A. Verma, S. Srivastava and V. M. Rotello, *Chem Mater*, 2005, **17**, 6317-6322.
28. K. S. Mayya, V. Patil and M. Sastry, *Langmuir*, 1997, **13**, 3944-3947.
29. S. Si, M. Raula, T. K. Paira and T. K. Mandal, *Chemphyschem*, 2008, **9**, 1578-1584.
30. Y. Tao, Y. H. Lin, J. S. Ren and X. G. Qu, *Biomaterials*, 2013, **34**, 4810-4817.
31. S. Z. Nergiz and S. Singamaneni, *Acs Appl Mater Inter*, 2011, **3**, 945-951.
32. J. J. Storhoff, R. Elghanian, R. C. Mucic, C. A. Mirkin and R. L. Letsinger, *J Am Chem Soc*, 1998, **120**, 1959-1964.
33. F. Canaveras, R. Madueno, J. M. Sevilla, M. Blazquez and T. Pineda, *J Phys Chem C*, 2012, **116**, 10430-10437.
34. C. Wang, J. Q. Zhuang, S. Jiang, J. Li and W. S. Yang, *J Nanopart Res*, 2012, **14**.
35. R. R. Arvizo, O. R. Miranda, M. A. Thompson, C. M. Pabelick, R. Bhattacharya, J. D. Robertson, V. M. Rotello, Y. S. Prakash and P. Mukherjee, *Nano Lett*, 2010, **10**, 2543-2548.
36. J. M. Chen, J. A. Hessler, K. Putchakayala, B. K. Panama, D. P. Khan, S. Hong, D. G. Mullen, S. C. DiMaggio, A. Som, G. N. Tew, A. N. Lopatin, J. R. Baker, M. M. B. Holl and B. G. Orr, *J Phys Chem B*, 2009, **113**, 11179-11185.
37. Y. C. Han, X. Y. Wang, H. L. Dai and S. P. Li, *Acs Appl Mater Inter*, 2012, **4**, 4616-4622.
38. R. S. Kass and D. S. Krafte, *J Gen Physiol*, 1987, **89**, 629-644.
39. N. Mahapatra, S. Datta and M. Halder, *Journal of Photochem and Photobiol A: Chem*, 2014, **275**, 72-80.
40. A. N. Shipway, M. Lahav, R. Gabai and I. Willner, *Langmuir*, 2000, **16**, 8789-8795.
41. T. Huang, F. Meng and L. M. Qi, *J Phys Chem C*, 2009, **113**, 13636-13642.
42. L. A. Li, C. F. Ke, H. Y. Zhang and Y. Liu, *J Org Chem*, 2010, **75**, 6673-6676.
43. V. T. Liveri, G. Cavallaro, G. Giammona, G. Pitarresi, G. Puglisi and C. Ventura, *Thermochim Acta*, 1992, **199**, 125-132.
44. P. Xiao, Y. Dudal, P. F. X. Corvini and P. Shahgaldian, *Polym Chem-Uk*, 2011, **2**, 120-125.
45. H. Mwakibete, R. Cristantino, D. M. Bloor, E. Wynjones and J. F. Holzwarth, *Langmuir*, 1995, **11**, 57-60.
46. J. Aguiar, P. Carpena, J. A. Molina-Bolivar and C. C. Ruiz, *J Colloid Interf Sci*, 2003, **258**, 116-122.

Table of Contents (TOC)

Easy and economical protocol for the reversible LSPR tuning of Ag NPs through cyclodextrin-induced self-aggregation and color fading, followed by surfactant-induced dissemination of self-assembly and consequent color reappearance.